

New coherent states in periodic arrays of ultrasmall Josephson junctions

Laurence Jacobs

*Center for Theoretical Physics, Laboratory for Nuclear Science and Department of Physics,
Massachusetts Institute of Technology, Cambridge, Massachusetts 02139*

Jorge V. José

*Service de Physique Théorique, Institut de Recherche Fondamentale de la Commissariat à L'Énergie Atomique,
Centre d'Études Nucléaires de Saclay, 91190 Gif-Sur-Yvette, France
and Department of Physics, Northeastern University, Boston, Massachusetts 02155**

M. A. Novotny

IBM Bergen Scientific Centre, Allégaten 36, N-5007 Bergen, Norway

A. M. Goldman

School for Physics and Astronomy, University of Minnesota, Minneapolis, Minnesota 55455

(Received 30 November 1987; revised manuscript received 14 April 1988)

An extensive study of the thermodynamics of a two-dimensional periodic array of ultrasmall Josephson junctions with and without a transverse magnetic field is presented. A quantum Monte Carlo algorithm is introduced to study a model that includes the Josephson energy, E_J , as well as the charging energy, E_c , contributions. The superfluid density, internal energy, and specific heat for different lattice sizes and numbers of Monte Carlo simulation sweeps are studied as a function of the ratio $\alpha = E_c/E_J$, the temperature and the magnitude of the magnetic field. When $\alpha \neq 0$, it is found that as the temperature is lowered the model has two phase transitions. First, a second-order Berezinskii-Kosterlitz-Thouless (BKT) transition is renormalized by the quantum fluctuations represented by a finite α . Below this BKT transition the system has long-range phase coherence; thus it is a state with zero resistance. At lower temperatures, a first-order phase transition appears which is entirely due to the quantum fluctuations that nucleate vortex excitations. Below this "quantum induced transition" (QUIT), the model still has a finite but diminished superfluid density, thus indicating that the QUIT is between two different zero-resistance states, one dominated by thermal fluctuations and the other by quantum fluctuations. A QUIT is found to be more pronounced in the case where there is a magnetic field. The case studied here corresponds in the classical limit to the fully frustrated state. Finally, we discuss the physical properties of this new low-temperature phase as well as the necessary conditions to test this prediction experimentally.

I. INTRODUCTION

Considerable attention has been focused recently on new effects that possibly may be seen in arrays of ultrasmall Josephson junctions, due to charging energy effects. In a recent series of publications, we have suggested that a transition from a usual superconducting state to a new coherent state dominated by zero-point quantum fluctuations may be observed in these systems.^{1,2} The conjectured phase transition has arisen from the studies of the thermodynamic properties of periodic arrays of Josephson junctions with very small capacitances (say from 10^{-13} to 10^{-15} F). The model studied considers the competition between the Josephson coupling energy E_J and the charging energy E_c between junctions. It was found that as a function of temperature for

$$\alpha = E_c/E_J, \quad (1.1)$$

different from zero, the system undergoes a low-temperature *first-order* phase transition.¹ This quantum (fluctuation-) induced (phase) transition (QUIT), is a transition between two different superconducting states as

measured by their nonzero superfluid density. More recently, we have found that a constant transverse magnetic field has a significant effect on the properties of a QUIT.²

The purpose of this paper is to give a detailed presentation of those results as well as the discussion of new ones. The approach is based on Feynman's imaginary-time representation of the corresponding quantum partition function.³ The evaluation of the appropriate thermodynamic averages is done using a quantum Monte Carlo (QMC) algorithm suitably tailored for the problem of interest. The actual representation of the discrete path integral studied in our simulations is obtained after a series of duality transformations that are discussed in the main body of the paper.

Arrays of Josephson junctions have been and are being extensively studied. Periodic arrays are made by using modern photolithographic techniques. Their physical properties are being studied extensively in the large-capacitance regime.⁴ The small junctions needed to see the effects described here are yet to be made, but at the end of the paper we discuss how they could be fabricated with the present photolithographic state of the art.

Another type of Josephson junction array that has been studied more extensively is that of granular materials in the dielectric regime, where the grain sizes can be very small, and thus have significant charging energy effects.⁵ The effects of the strong disorder present in these systems have to be considered carefully, however.

Typically, in these arrays of Josephson junctions, the measured resistance R as a function of temperature T shows a monotonic decreasing behavior below the bulk superconducting temperature T_{c0} . The temperature at which the material finally becomes superconducting, i.e., $R=0$, is T_c . The qualitative interpretation of this behavior is that near T_{c0} the superconductors forming the junctions develop superconducting fluctuations as in a bulk material. However, since the grains are of finite size, a true superconducting phase transition cannot take place. Nonetheless, one can associate a Ginzburg-Landau order parameter to each grain. A Josephson coupling between grains appears below T_{c0} , and eventually at T_c the system establishes long-range phase coherence, i.e., $R=0$. The width $T_{c0}-T_c$ depends on the spread of values of the E_J 's. When the superconductors making the junctions are ultrasmall, the width $T_{c0}-T_c$ is affected since then the Josephson current is impeded by the static electric field between them and thus T_c decreases with increasing E_c . The value of E_c can increase to the extent that long-range phase coherence is no longer possible.

Once the zero-resistance state has been established, if the charging energy is non-negligible, new things can happen at low temperature where the thermal fluctuations are no longer dominant and the quantum or zero-point fluctuations become significant. Within the context of a mean-field (MF) theory, Simanek⁶ and Efetov⁷ found reentrant phase transitions, i.e., a normal-superconducting-normal scenario as T decreases. Other MF calculations, self-consistent harmonic approximations, and variational calculations do not find a reentrant transition.^{8,9} Recent improvements of the MF within the Oguchi approximation, while not leading to a reentrant transition, did find evidence for a short-range phase enhancement due to the presence of the charging energy.¹⁰ All these analyses have had the feature that dimensionality does not play a significant role, and thus their regime of applicability would be expected to be that of higher-dimensional systems. An exception is the two-dimensional scaling analysis of Doniach.¹¹ He studies a coarse-grained approximation of the lattice model, in imaginary time, studied by Simanek and Efetov. Doniach uses the fact that the model at zero temperature becomes an anisotropic three-dimensional XY model, with α playing the role of temperature. Thus there is a critical value of α , say α_c , such that there is a "long-range order" below α_c and disorder above α_c . At high temperatures the model behaves like a two-dimensional (2D) XY model, and thus a Berezinskii-Kosterlitz-Thouless phase transition should ensue. The question is what happens for intermediate temperatures. Within a scaling analysis Doniach does not find any signature for a reentrant transition as discussed by either Simanek or Efetov.

A study of an explicitly two-dimensional model within the semiclassical approximation was considered by one of

us.³ The Wentzel-Kramers-Brillouin (WKB) limit corresponds to high temperatures. By expanding the Hamiltonian of the model in powers of $\hbar/k_B T$ (with k_B being Boltzmann's constant and $\hbar = h/2\pi$ with h being Planck's constant), the problem was reduced to that of a 2D XY model but with a Josephson coupling constant modified by E_c . From an analysis of the corresponding renormalization-group (RG) equations, it was found that T_c decreases monotonically with α , as expected, but with all the critical exponents of the classical XY model (i.e., when $\alpha=0$) unchanged. Although the changes are mainly quantitative, these modifications have proven to be necessary to fit the experimental data on granular NbN granular superconductors.¹²

The same WKB analysis found that at low temperatures the RG recursion equations become unstable, which could be the signature of a low-temperature instability. The instability was conjectured to be a reentrant-type transition, although of a different nature than the one considered by Simanek and Efetov, since the two dimensionality of the excitations in the system are essential. Serious questions about the existence of the low-temperature instability arise since the region of validity of the WKB approach used is clearly out of the temperature region where the instability would appear. Thus, a non-perturbative non-MF approach is needed to ascertain with more confidence if indeed there is a low-temperature instability due to the presence of quantum fluctuations in Josephson junctions arrays, and to understand its properties. With this idea in mind, we have carried out QMC nonperturbative calculations to resolve these questions.

From the QMC results presented in this paper it is now clear that there is indeed a low-temperature quantum-induced phase transition. This QUIT, however, has properties that had not been previously surmised. The QUIT is from *normal* to S_1 (*superconducting 1*) and then to S_2 (*superconducting 2*). The normal to S_1 transition is of the *second-order* Berezinskii-Kosterlitz-Thouless (BKT) type¹³ with an α -dependent critical temperature with a qualitative behavior as found by the WKB analysis, but quantitatively different. The critical exponents remain universal for sufficiently small values of α . The transition from S_1 to S_2 is of *first order* between two states with finite superfluid density, that of 1 being larger than that of 2. In some dimensionless units defined below, if $T_c \sim 1$ then $T_{\text{QUIT}}(\alpha=0.3) \sim 0.03$, a low temperature indeed. The superfluid density differences in the two states are quite small, $\Delta\rho \sim 0.02$. Of significance is the fact that the specific heat that has a maximum of order one around T_c , becomes six times larger around T_{QUIT} . Thus if c_v can be measured, it should give a clear signature of the QUIT.

To understand the properties of this QUIT further we proceed to consider the effects of an external magnetic field. The problem of an array of Josephson junctions in a magnetic field, without charging effects, has been studied extensively in recent years.¹⁴ The problem is rather subtle in its properties since it depends intrinsically on the number-theoretic nature (rational or irrational) of the "frustration" parameter

$$f = \Phi/\Phi_0, \quad (1.2)$$

where Φ is the magnetic flux through an elementary plaquette in the lattice and Φ_0 is the fundamental quantum of flux ($\Phi_0 = 2.07 \times 10^{-7}$ G cm²). Even for a square lattice the behavior of the critical temperature as a function of f has the Hofstadter-Cantor setlike structure.¹⁵ Correspondingly, the geometrical properties of the lattice can be “seen” in the complicated response of the system at $T_c(f)$. The problem when $f = \frac{1}{2}$ is particularly interesting since it corresponds to the fully frustrated case studied first by Villain and others,¹⁶ and within the superconducting context by Teitel and Jayaprakash.¹⁷ The main result, for $f = \frac{1}{2}$, is that there is a decrease of the superfluid density with a lower critical temperature $T_c(f = \frac{1}{2}, \alpha = 0) \sim 0.45$. The nature of the phase transition is still unclear since the model shows XY BKT-type properties as well as an Ising diverging specific heat.¹⁴ In an interesting analysis by Berge *et al.* the amount of frustration was varied by changing one of the coupling strengths E_J in a plaquette.¹⁸ Their results show that in this case there are two transitions as a function of temperature. The low-temperature transition being Ising-like while the high-temperature transition is XY . The question remains as to the real nature of the transition in the homogeneous system with $f = \frac{1}{2}$, although recent experimental results give strong evidence for having an XY -like transition.¹⁹

Here, as a first nontrivial step we consider the $f = \frac{1}{2}$ case with nonzero charging energy. We do not analyze the real nature of the high-temperature phase transition except to measure its α dependence, which, as in the $f = 0$ case, is a monotonically decreasing function of α , although with a smaller slope. It is the low-temperature phase that interests us most here. There we find a QUIT, but with properties which are noticeably clearer than in the $f = 0$ case. First, the critical temperature is $T_{\text{QUIT}}(f = \frac{1}{2}, \alpha = 0.5) \sim 0.12$, an order of magnitude larger than in the $f = 0$ case. Also of importance is the fact that $\Delta\rho(f = \frac{1}{2}, \alpha = 0.5) \sim 0.1$, i.e., about 30 times larger than in the $f = 0$ case. We observe clear signatures of hysteresis loops, thus indicating that we have a stronger first-order transition. Although these results may appear as just an amplification of the $f = 0$ results, as surmised for the $\alpha = 0$ and $f = \frac{1}{2}$ case, the physics is sufficiently different to need a separate analysis. We shall discuss these points in more detail in the main body of the paper.

The contents of the paper are divided into seven sections and one appendix. In Sec. II the models studied are introduced. We also discuss most of the additions to the models that would make them more realistic, but which we leave out at this time to make the analysis feasible. Section III discusses the mapping of the operator representation of the quantum-mechanical models into their Feynman imaginary-time path integral. There we stress the important properties of this representation and the limits at which we can recover the true quantum behavior of the model. Using duality transformations, we arrive at the explicit expressions for the partition function used in the quantum Monte Carlo (QMC) simulations. As a useful test of the numerical algorithm developed to treat this problem, we consider the “zero-dimensional” case of a single rotor using an exact finite-dimensional transfer-matrix analysis. This study illustrates clearly the care

that has to be taken to obtain true quantum behavior at low temperatures. This transfer-matrix analysis is given in the Appendix. In Sec. IV the QMC algorithm is introduced and its advantages and shortcomings are discussed. The algorithm is tested against the known solutions in the zero-dimensional and in the high-temperature two-dimensional cases. It is here where we make explicit why these calculations, to be reliable, have required large amounts of supercomputer time. All results presented in this paper were obtained from simulations run on Cray-XMP and Cray2 computers. Section V presents the results together with a discussion of their physical significance. Section VI discusses the fabrication of periodic arrays of Josephson junctions such that the predictions made in this paper may be tested. In Sec. VII we give a discussion of the results in terms of the known behavior, for the $f = 0$ and $f \neq 0$ models, at $T = 0$ and close to $T_c(f)$. We propose a plausible phase diagram which is consistent with the results of Sec. IV.

II. DEFINITION AND PROPERTIES OF THE MODELS STUDIED

Our goal is to understand the thermodynamic properties of two-dimensional arrays of ultrasmall Josephson junctions (JJ). An example of an array of JJ consists of metallic grains embedded in an insulating matrix. These granular films are formed by various deposition techniques. Depending on the amount of metal deposited on appropriate substrates, one can separate three distinct concentration regimes by their conduction mechanism processes. When the amount of metal is large, i.e., when the volume occupied by the insulating inclusions is small, the specimens have metallic behavior but with conductivities $\sigma_g \ll \sigma_C$, with σ_g being the inhomogeneous material conductivity and σ_C the crystal conductivity in the bulk metal. Also, the superconducting Ginzburg-Landau coherence length $\xi_g \ll \xi_C$, and the London penetration depth $\lambda_g \gg \lambda_C$, thus making these inhomogeneous systems strong type-II superconductors. When the amount of metal is close to the percolation limit, the conductivity has percolative as well as variable-range hopping contributions.⁵

When the insulating regions occupy a larger volume, conductivity will be dominated exclusively by thermally activated and quantum-mechanical tunneling processes. It is this *dielectric regime*, when the grains have dimensions from tens to a few hundred angstroms, that is of interest in the present discussion. If the metal in the bulk is superconducting, a zero-resistance state is reached for certain concentrations of metals in the granular systems. This is because of the long-range phase-coherent (LRPC) state due to the Josephson couplings established between the grains.

One can expect that this dielectric regime can also be created experimentally by fabricating periodic arrays of JJ using modern photolithographic techniques. As of now, these types of arrays have not been made. However, there are a number of recent advances which may permit the fabrication of these devices using present state-of-the-art technology. We discuss these works and their pos-

sibilities in Sec. VI.

Typically, in these systems the measured resistance R shows a two-stage mechanism as the temperature T decreases. A monotonic decrease starts at temperatures around the bulk superconducting (SC) temperature, T_{c0} . The zero-resistance state is reached at a lower temperature, T_c , at which $R=0$. The present interpretation of this behavior is as follows: Around T_{c0} the grain develops SC fluctuations. Since they are of finite size, however, LRPC cannot be established. If the typical size of the grains d is smaller than the bulk ξ_{GL} , one can associate a Ginzburg-Landau order parameter with each grain,

$$\Psi_i = |\Psi_i| e^{i\phi_i}, \quad (2.1)$$

where $i = \sqrt{-1}$ and i stands for a two-dimensional position vector and ϕ_i is a phase constrained to lie in the interval $\phi_i \in [0, 2\pi]$. The fluctuations of the magnitude of the order parameter are larger for temperatures just below T_{c0} . However, closer to T_c the magnitude fluctuations are very small and the fluctuations in ϕ_i become dominant. Thus, around and below T_c the grains become Josephson coupled, with the coupling energy

$$\mathcal{H}_J = \sum_i E_J(i+1, i) [1 - \cos(\phi_{i+1} - \phi_i)]. \quad (2.2)$$

The Josephson coupling constant $E_J(i+1, i)$ is also an explicit function of temperature, the superconducting gap $\Delta(T)$, and the normal-state resistance between grains $R(i+1, i)$:

$$E_J(i+1, i) = \frac{\hbar \pi \Delta(T)}{4e^2 R(i+1, i)} \tanh \left[\frac{\beta \Delta(T)}{2} \right]. \quad (2.3)$$

Here e is the electronic charge. Taking E_J as a constant, the thermodynamics associated with \mathcal{H}_J is that of the 2D classical XY model with a Berezinskii, Kosterlitz, and Thouless (BKT) vortex-unbinding transition. The BKT scenario leads to universal predictions that have been confirmed in several experiments. For periodic systems, the temperature dependence can be ignored in the theoretical analysis and included when comparing with experimental results.²⁰ In general, for a granular system, $E_J(i, +1, i)$ will be a random variable. For small amounts of randomness, it has been shown that the thermodynamic properties of this model are like those of the BKT scenario with renormalized coupling constants, but with the same universal exponents. The case of large amounts of disorder is not yet understood.

Of importance for the present study is the fact that the grains are small. In this case, the charging energy associated with the grains becomes relevant and thus will compete against the Josephson energy which tries to establish a superconducting current between grains. The charging energy contribution to the total energy between two superconductors separated by a thin insulating region was considered by Anderson in the context of the first Josephson junctions and within the context of granular materials by Abeles. A general form for the charging energy Hamiltonian is

$$\mathcal{H}_e = \frac{e^2}{2} \sum_i \hat{n}_{i+1} C_{i+1, i}^{-1} \hat{n}_i, \quad (2.4)$$

where \hat{n}_i is the operator that measures the number of Cooper pairs transferred between grains, and $C_{i+1, i}^{-1}$ is the inverse of the capacitance matrix. This matrix can have a long-range contribution; however, due to Coulomb screening effects we can take it as a nearest-neighbor matrix. For a granular material this matrix is also a random variable whose randomness is not completely independent of that of $E_J(i+1, i)$. In Eq. (2.4) quasiparticle charging effects are not included.

The variables ϕ_i and \hat{n}_i are canonically conjugate and satisfy the commutation relations,

$$[\hat{n}_k, \phi_j] = -i \delta_{k, j}. \quad (2.5)$$

From these commutation relations it is clear that when the fluctuations in the phase difference between the grains $\Delta\phi \ll 1$, the Josephson current is well established since from Heisenberg's uncertainty principle $\Delta n \gg 1$. When $\Delta\phi \sim \Delta n$ the charge in the grains is well defined and thus the charging energy becomes important in determining if there is LRPC.

An understanding of the superconducting properties of a material results from studying its response to an external magnetic field. Adding a transverse magnetic field leads to the Hamiltonian

$$\mathcal{H}_J = \sum_i E_J(i, i+1) [1 - \cos(\phi_{i+1} - \phi_i + f_{i+1, i})] \quad (2.6)$$

with

$$f_{i+1, i} = \frac{2\pi}{\Phi_0} \int_{i+1}^i \vec{A} \cdot d\vec{l} \quad (2.7)$$

where \vec{A} is the magnetic vector potential with $\vec{H} = \vec{\nabla} \times \vec{A}$ and $f = \sum_p f_{i+1, i}$ is the frustration parameter defined in Sec. I with \sum_p the sum around a plaquette. Equation (2.6) with E_J constant has been studied extensively. In all our calculations with $f \neq 0$ we use the gauge

$$\vec{A} = (0, Hx, 0).$$

The thermodynamics of the model is rather complicated depending intrinsically on the lattice geometry and the rationality of f . The Hamiltonian being periodic in f needs to be studied only for the interval $0 \leq f \leq \frac{1}{2}$. For the particular value $f = \frac{1}{2}$, the model corresponds to the fully frustrated XY model first considered by Villain.¹⁶ The nature of the phase transition is a source of controversy since the model has $U(1)$ symmetry from the rotational invariance and $Z(2)$ or Ising symmetry from the f -induced invariance. Numerically it is found that the model has a finite superfluid density at the lower critical temperature while the specific heat shows a logarithmiclike divergence around T_c ($f = \frac{1}{2}$).¹⁷ Recent experiments in a periodic array of proximity-effect Josephson junctions in a field of $f = \frac{1}{2}$ show all the characteristics of a BKT transition, including the square root exponentially increasing correlation length above T_c ($f = \frac{1}{2}$).¹⁹

An important condition to be able to see experimentally a BKT-type transition is that the contributions from the screening currents should be negligible. Otherwise, the logarithmic interaction between vortices would be

screened and no topological phase transition would be observable. The quantum nature of the phase, and specifically the effects of dissipation, seem to be important in explaining the conditions for onset of superconductivity in recent experiments on granular ultrathin films.²¹ From these experimental results, it has been suggested that there is a universal value of the sheet resistance independent of the material, below which the system becomes superconducting. The universal resistance takes the value around $R_c = h/4e^2 \sim 6 \text{ k}\Omega$. We will not treat the effects of dissipation in this paper and leave it for a future publication.

Here we are mainly interested in the questions of stability of the superconducting or LRPC state against quantum fluctuations with and without an external magnetic field. At the present moment we cannot include all the effects pertaining to a more realistic description of a granular material with ultrasmall grains. Hence, we make approximations to the models described above to isolate the effects related to the charging energy in a periodic lattice.

We start by considering the nonrandom case, i.e., $E_J(i+1, i) = E_J = \text{const}$, and the capacitance matrix will be taken constant as well and only with a diagonal contribution $C(i+1, i) = C(i, i) = C = \text{const}$. One would expect, based on general electrostatic considerations about the positivity of the electrostatic energy, that since $|C_{i+1, i}| \geq C_{i, i} = C$ the main effects may come from the diagonal term. However, the question remains if the off-diagonal contributions may in fact affect the phase diagram of the model. This is an approximation that has been made often, but its effects in two dimensions are not fully understood due to the fact that technically it leads to a more difficult model to study. This nonrandom approximation corresponds to a periodic array of JJ with small capacitances, and thus we expect our results to apply directly to those systems. On the other hand, taking the coupling constants as nonrandom may be justified when the randomness is small and when looking at the long-range properties of the granular system.

The model studied in this paper is finally given by the periodic Hamiltonian:

$$\mathcal{H} = \sum_i \left[E_J [1 - \cos(\phi_{i+1} - \phi_i + f_{i+1, i})] + \sum_i \frac{e^2}{2C} \frac{\partial^2}{\partial \phi_i^2} \right]. \quad (2.8)$$

Here we have used $\hat{n}_i = -i(\partial^2/\partial \phi_i^2)$ which follows from Eq. (2.5). Although this Hamiltonian is a simplification of the general case, it is nonetheless a highly nontrivial model. It represents a quantum many-body problem in which the dimensionality plays a crucial role.

The thermodynamic properties associated with \mathcal{H} are obtained from the partition function

$$\mathcal{Z}_Q = \text{Tr} e^{-\beta \mathcal{H}}, \quad (2.9)$$

where Tr stands for the quantum-mechanical trace. In the next section we transform \mathcal{Z}_Q into its Feynman path-integral representation which permits a numerical evaluation for a full range of parameters.

III. IMAGINARY TIME REPRESENTATION OF \mathcal{Z}_Q

To evaluate \mathcal{Z}_Q in two dimensions and in the operator representation seems rather complicated. Thus we choose to study \mathcal{Z}_Q in its imaginary-time or Feynman path-integral representation which is amenable to Monte Carlo simulations. Since we want to study the physics of \mathcal{Z}_Q at very low temperatures, the regime where quantum fluctuations are dominant, we need to be sure that the numerical answers obtained are the correct ones in this regime. Thus we need to find the conditions under which we find the real quantum behavior of this model. Since the quantum fluctuations are directly related to the kinetic-energy contribution to \mathcal{H} , we begin this section by considering the thermodynamics of the kinetic-energy term. In this limit ($E_J = 0$), the model reduces to that of N -independent rotors, the answer to which is found in any elementary quantum-mechanics book. It is thus instructive to study this simple model to ascertain the limits of validity of the numerical results obtained from the simulations.

At the end of this section we proceed to consider the full model including the E_J and $f_{i, i+1}$. We choose to study the full model in its dual representation which makes the symmetry explicit between high and low temperatures, i.e., thermal and quantum fluctuations dominated regimes, respectively.

A. Single-rotor case

The $E_J = 0$ partition function decouples into a set of independent rotors each of which has

$$\mathcal{Z}_{\mathcal{R}} = \text{Tr} \left[\exp \left[-E_c \beta \frac{\partial^2}{\partial \phi^2} \right] \right], \quad (3.1)$$

where

$$E_c = \frac{e^2}{2C}. \quad (3.2)$$

The normalized eigenfunctions and eigenvalues of the rotor Hamiltonian are

$$|\phi_m\rangle = \frac{1}{\sqrt{2\pi}} e^{im\phi},$$

$$\epsilon_m = \frac{1}{2} E_c m^2,$$

with m an integer. Therefore,

$$\mathcal{Z}_{\mathcal{R}} = \sum_{m=-\infty}^{\infty} \exp(-\frac{1}{2} \beta E_c m^2). \quad (3.3)$$

We would like to recover this result in the limit $\frac{1}{2} \beta E_c \gg 1$ within the context of the path-integral representation using a Monte Carlo algorithm. $\mathcal{Z}_{\mathcal{R}}$ can be obtained as usual from the trace of the matrix elements of the time evolution operators $\hat{U} = e^{-\beta \mathcal{H}}$:

$$\mathcal{Z}_{\mathcal{R}} = \int_0^{2\pi} d\phi \langle \phi | \hat{U}(\tau, \tau) | \phi \rangle, \quad (3.4)$$

where

$$\langle \phi_2 | \hat{U}(\tau_2, \tau_1) | \phi_1 \rangle = \int_0^{2\pi} \prod_{k=1}^{L_\tau-1} d\phi(\tau_k) \prod_{k=1}^{L_\tau} \langle \phi(\tau_k) | \hat{U}(\tau_k, \tau_{k-1}) | \phi(\tau_{k-1}) \rangle. \quad (3.5)$$

Here k is an integer, L_τ is the number of time slices in the imaginary-time axis,

$$\tau_k = \tau_1 + k\epsilon$$

with ϵ spacing between time slices, and

$$L_\tau \epsilon = \beta \hbar. \quad (3.6)$$

The boundary conditions are

$$\phi(\tau = \tau_1) = \phi_1, \quad \phi(\tau = \tau_2) = \phi_2. \quad (3.7)$$

The quantization condition is given by the periodicity requirement,

$$\phi(\tau + \beta \hbar) = \phi(\tau). \quad (3.8)$$

For the problem at hand the matrix elements of \hat{U} are

$$\begin{aligned} \langle \phi(\tau_k) | \hat{U}(\tau_k, \tau_{k-1}) | \phi(\tau_{k-1}) \rangle &= \frac{1}{2\pi} \sum_{m_k, m_{k-1}} \langle \phi_k | m_k \rangle \langle m_k | \hat{U}(\tau_k, \tau_{k-1}) | m_{k-1} \rangle \langle m_{k-1} | \phi_{k-1} \rangle \\ &= \frac{1}{2\pi} \sum_{m_k} \int_0^{2\pi} d\phi_k \int_0^{2\pi} d\phi_{k-1} \exp[i m_k (\phi_{k-1} - \phi_k) - \frac{1}{2} \beta E_c m_k^2], \end{aligned} \quad (3.9)$$

where we used the orthogonality relation $\langle m_k | m_{k-1} \rangle = \delta_{k, k-1}$. Using Eqs. (3.5), (3.6), and (3.11), the partition function reads

$$\mathcal{Z}_{\mathcal{R}} = (2\pi)^{-L_\tau/2} \int_0^{2\pi} \prod_{k=1}^{L_\tau} \sum_{m(\tau_k)} \exp \left[\sum_{k=1}^{L_\tau} \left[i m(\tau_k) [\phi(\tau_{k-1}) - \phi(\tau_k)] - \beta \frac{E_c}{2L_\tau} m^2(\tau_k) \right] \right] d\phi(\tau_k). \quad (3.10)$$

One can transform this equation to a more convenient form using the Poisson identity,

$$\sum_{n=-\infty}^{\infty} f(n) = \sum_M \int_{-\infty}^{\infty} f(X) e^{2\pi i M X} dX. \quad (3.11)$$

Hence $\mathcal{Z}_{\mathcal{R}}$ becomes

$$\mathcal{Z}_{\mathcal{R}} = \left(\frac{L_\tau}{\beta E_c} \right)^{L_\tau/2} \int_0^{2\pi} \prod_{k=1}^{L_\tau} \sum_{M(\tau_k, \tau_{k-1})} d\phi(\tau_k) \exp \left[- \frac{L_\tau}{2\beta E_c} \sum_{k=1}^{L_\tau} [\phi(\tau_{k+1}) - \phi(\tau_k) + 2\pi M(\tau_{k+1}, \tau_k)]^2 \right]. \quad (3.12)$$

The integer link variables $M(\tau_{k+1}, \tau_k)$ are defined between the sites k and $k+1$. The appearance of these variables come directly from the fact that ϕ is constrained to lie in the interval $[0, 2\pi]$, and thus is essential to the study discussed here. Since it is difficult to do simulations simultaneously for the integer and angular variables, it is more convenient to rewrite $\mathcal{Z}_{\mathcal{R}}$ in the form

$$\mathcal{Z}_{\mathcal{R}} = \left(\frac{L_\tau}{\beta E_c} \right)^{L_\tau/2} \int_0^{2\pi} \prod_{k=1}^{L_\tau} d\phi(\tau_k) \exp \left[- \sum_{k=1}^{L_\tau} \frac{2L_\tau}{\beta E_c} \{1 - \cos[\phi(\tau_{k+1}) - \phi(\tau_k)]\} \right], \quad (3.13)$$

which is exact in the limit that $2L_\tau/\beta E_c \gg 1$, which is, in fact, our limit of interest. This expression for $\mathcal{Z}_{\mathcal{R}}$ is reminiscent of the partition function for the classical XY model. However, the limits and the boundary conditions under which this model has to be studied lead to different answers. To see this, we need to show under what conditions we recover the exact solution given in Eq. (3.3).

Using the identity

$$\int_0^{2\pi} \frac{dX}{2\pi} \exp \left[-iMX - \frac{L_\tau}{\beta E_c} [1 - \cos(X)] \right] = e^{L_\tau/\beta E_c} I_M \left(\frac{L_\tau}{\beta E_c} \right), \quad (3.14)$$

where I_M is the modified Bessel function of order M , $\mathcal{Z}_{\mathcal{R}}$ can be expressed as

$$\mathcal{Z}_{\mathcal{R}} = \left(\frac{L_\tau}{\beta E_c} \right)^{L_\tau/2} \sum_{M(\tau_{k+1}, \tau_k)} \int_0^{2\pi} \prod_{k=1}^{L_\tau} d\phi(\tau_k) \exp \{ i M(\tau_{k+1}, \tau_k) [\phi(\tau_{k+1}) - \phi(\tau_k)] \} e^{-L_\tau/\beta E_c} I_{M(\tau_{k+1}, \tau_k)} \left(\frac{L_\tau}{\beta E_c} \right). \quad (3.15)$$

From the asymptotic limit,

$$I_M \left(\frac{L_\tau}{\beta E_c} \right) \sim e^{-M^2 \beta E_c / L_\tau}, \quad (3.16)$$

valid when $L_\tau / \beta E_c \gg 1$, we recover the quantum-mechanical answer given in Eq. (3.3). This reasoning makes it clear that in order to obtain the quantum limit from $Z_{\mathcal{R}}$ we need to take the $L_\tau \rightarrow \infty$, as well as the $\epsilon \rightarrow 0$ limits, i.e., the continuum limit,

$$\lim_{\epsilon \rightarrow 0} \lim_{L_\tau \rightarrow \infty} L_\tau \epsilon = \beta \hbar. \quad (3.17)$$

Formally, one usually writes this limit as a path integral,

$$Z_{\mathcal{R}} = \int d[\phi(\tau)] \exp \left[-\frac{1}{\hbar} \frac{\hbar^2}{E_c} \int_0^{\beta \hbar} \left(\frac{d\phi}{d\tau} \right)^2 d\tau \right]. \quad (3.18)$$

Implicit in this expression are the conditions given in Eqs. (3.7) and (3.8), plus the fact that there is a coefficient that depends explicitly on L_τ . Since we are interested in the thermodynamic properties related to $Z_{\mathcal{R}}$, we need to take derivatives with respect to β , which appears in the coefficient, as well as in the limits of integration of the kinetic energy.

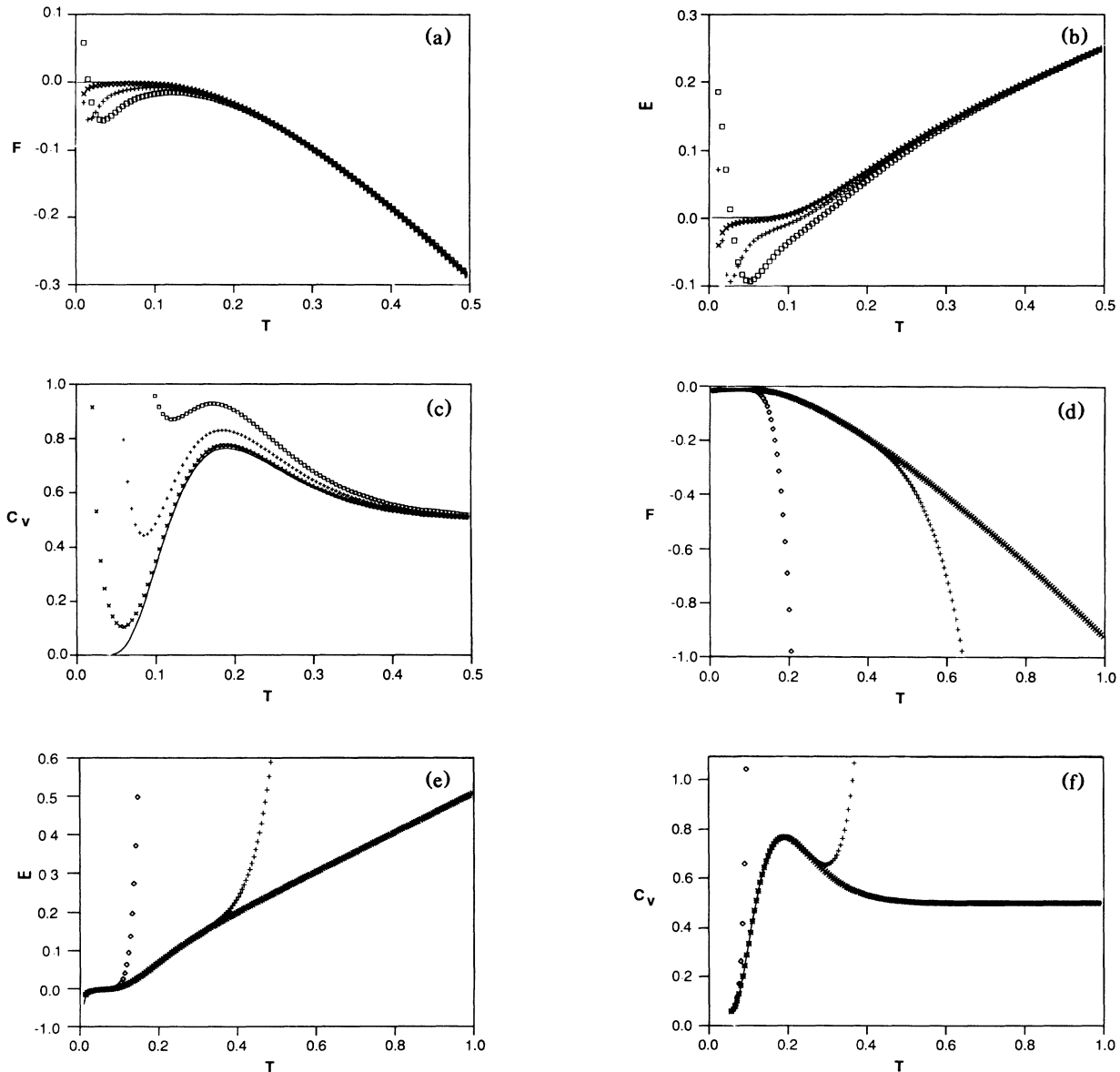


FIG. 1. The free energy, internal energy, and specific heat are shown for the uncoupled rotor problem, $E_J = 0$. (a), (b), and (c) show the effect of various values of L_τ ($\square = 50$; $+$ = 100; \times = 500; continuous curve is the infinite L_τ limit), for the model with the phase ϕ_l having a continuous $U(1)$ symmetry. (d), (e), and (f) are for $L_\tau = 10^3$, with the phases restricted to the elements of various Z_N subgroups of the $U(1)$ symmetry of the model N ; $\diamond = 50$; $+$ = 100; \times = 500; continuous line exact result. See the text for a full discussion.

Since the Monte Carlo simulations for the full model, to be discussed later, are by force carried out for finite L_τ and for a subgroup of $U(1)$, Z_N , we need to obtain criteria for the minimum values that these parameters should have, as a function of α and β , such that the answers are the correct ones. In so doing we use different methods to evaluate $Z_{\mathcal{R}}$. First we evaluate analytically $Z_{\mathcal{R}}$ from Eq. (3.13) as a function of L_τ by using the identity of Eq. (3.14) and compare it with the exact result of Eq. (3.3). Figures 1(a), 1(b), and 1(c) show, respectively, the free energy, internal energy, and specific heat evaluated directly from Eq. (3.13) for different values of L_τ . From these figures we see that for high temperatures, such as near the BKT transition temperature, a small value of L_τ suffices while the study of low temperatures, as in the region of the QUIT temperature, large values ($L_\tau \sim 1000$) are needed to get the correct answers.

Figures 1(d), 1(e), and 1(f) show, respectively, the free energy, internal energy, and specific heat evaluated using the transfer-matrix technique discussed in the Appendix for $L_\tau = 10^3$ and with the phases $\phi \in [0, 2\pi]$ discretized into N equal angles. A trivial normalization factor of $\beta E_c/8$ was subtracted from the free energies to compare with the free energy from Eq. (3.3). This is a convenient approximation which permits evaluation of the partition function using a finite number of equally spaced angles. Figures 1(d), 1(e), and 1(f) show that while small values of N provide excellent approximations at low temperatures, at high temperatures larger N values are required to obtain adequate approximations. *This is opposite* of the classical plane-rotator model (see Ref. 22), where large- N values are required at low temperatures. It has been found for the classical XY model²² that $N \sim 12$ is enough to give accurate answers. Because we must have $L_\tau \geq 2$, we require N to be large at high temperatures in our model. We also require N to be large at temperatures much lower than those simulated in this paper, for the same reason that N must be large in the classical model at low temperatures. However, at the low temperatures simulated in this paper,

we are mainly limited by finite L_τ values and the magnitude of N does not present a problem. As seen from Fig. 1, in the quantum case $N \geq 5000$ gives accurate answers for all temperatures of interest in our case.

Because any nonzero coupling between rotators would provide additional paths for fluctuations, the graphs in Fig. 1 may be used to provide an approximate upper bound on the values of N and L_τ required to give an approximation to the exact values of the thermodynamic quantities over some temperature range. We used these curves as a guide for which values L_τ were required in different temperature regions. In addition, as discussed in the next section, we demanded that large enough values of L_τ be used so the errors were of a statistical nature rather than due to the approximation due to finite L_τ values.

The conclusion from the analysis of the thermodynamics of a single rotator problem is that to recover the true quantum answers at low temperatures we need to have $2L_\tau/\beta E_c \gg 1$, as well as having $N \geq 5000$. The former conditions will impose stringent requirements on the minimum lattice sizes on which to carry out the simulations to get reliable answers. Since we are interested in simulating a 2D quantum problem the conditions for convergence are less severe than those found in the 0D problem, but nonetheless still significant.

B. Duality representation of Z_Q

We can now consider the model of main interest in this paper. Adding the Josephson term to the partition function given in Eq. (3.13) is straightforward and we write the full partition function as

$$Z_Q = \left(\frac{L_\tau}{\beta E_c} \right)^{V/2} \int_0^{2\pi} d[\phi(\tau)] e^{-A[\phi(\tau)]} \quad (3.19)$$

with

$$A[\phi(\tau)] = \sum_{i,k} \left[\left(\frac{L_\tau}{\beta \alpha E_j} \right) \{1 - \cos[\phi(\tau_{k+1}) - \phi(\tau_k)]\} + \frac{E_j \beta}{L_\tau} \{1 - \cos[\phi_{i+1}(\tau_k) - \phi_i(\tau_k) + f_{i+1,i}(\tau_k)]\} \right], \quad (3.20)$$

where $V = L \times L \times L_\tau$. This representation of Z_Q makes evident an important physical symmetry between the kinetic (quantum) and the potential or Josephson (thermal) contributions. Since the most important contributions to the partition function come from the smallest terms in the action $A[\phi(\tau)]$, we see that the kinetic-energy term, for fixed L_τ , is multiplied by β^{-1} , and at low temperatures this term will become the most relevant one in the action. Similarly, since the Josephson term is multiplied by β , it is at high temperatures that this term will dominate the thermodynamics of the model. This ‘‘dual’’ symmetry, apart from having a clear physical meaning, will be exploited in the implementation of the QMC algorithm to be discussed in the next section.

In the way we have rewritten Z_Q we notice the following facts. We started with a 2D operator quantum prob-

lem and the result of writing Z_Q in the imaginary-time representation is that we now have to study a three-dimensional problem. In the limit of high temperatures the model approaches the two-dimensional classical behavior since $\beta \hbar \ll 1$. We note that for $f=0$, $\alpha \neq 0$ the model can be recast into the form of an anisotropic classical 3D XY model with α playing the role of temperature. The physics at $T=0$ and close to $T_{\text{BKT}}(\alpha)$ is clear, and thus the important question is to find the properties of the model in the intermediate temperature regime. The situation is less clear when $f \neq 0$, since the corresponding model has not been studied before.

In the next sections we present and discuss the results obtained from Monte Carlo simulation studies of the model given in Eqs. (3.19) and (3.20), in different parameter regions of interest.

IV. QUANTUM MONTE CARLO METHOD

The simulations carried out on the model defined in Eqs. (3.19) and (3.20) employed the standard Metropolis algorithm²³ on $L \times L \times L_\tau$ lattices with periodic boundary conditions in both spatial and imaginary-time directions. However, several modifications to this technique were used to optimize the efficiency of the algorithm. In particular, the reciprocal β dependence of the two terms in the action given in Eq. (3.20) was exploited. The lattice sizes and the statistics used will be discussed in the next section. Here we describe the algorithm and the thermodynamic quantities measured.

As mentioned above, at high temperatures the potential-energy term dominates while at low temperatures it is the kinetic-energy term that is most relevant. Both contributions are relevant for $\beta \sim 1$. This temperature dependence must be taken into account in the implementation of an efficient algorithm. At temperatures with $\beta \leq 1$, individual planes begin to disorder in such a way that disorder between adjacent planes along the τ axis does not increase since otherwise a strong Boltzmann suppression would ensue. For this reason the QMC updating was carried out in two stages. First an update of the angles in each of the L^2 columns in the τ direction was attempted by shifting all angles in a given column by the *same* amount using the standard Monte Carlo (MC) algorithm. At high temperatures (or small charging energy) angular configurations that do not have all angles the same in a given L_τ column are highly improbable. Hence the first QMC stage is necessary in this region. We then proceeded to update the $L^2 L_\tau$ angles in the lattice in the usual way. A similar improvement at very low temperatures, where individual planes tend to order (up to topologically stable defects), would entail updating all L^2 angles for a given "time slice" as well as updating individual angles. This procedure would unreasonably tax the numerical precision limitations inherent in this type of simulation, but in our work this third possibility is not necessary since for the temperature range considered here the two-stage MC procedure works reasonably well.

As mentioned before, rather than using the continuous

U(1) symmetry of the problem, to increase the computation speed we used a discrete \mathbb{Z}_N subgroup. For N sufficiently large, while not bearing on the physics, this approximation permits the use of look-up tables in the simulations. As demonstrated in the case of the single rotor model at low temperatures, the size of the \mathbb{Z}_N subgroup must be large to provide adequate results. We found that using $N = 5000$ at all temperatures gave good results. The angular width was varied continuously to allow for an angular change of the two QMC stages to keep the acceptance ratio in the range $0.2 \leq a \leq 0.3$. This prevents the problem present at the two extremes of acceptance ratio where the system tends to remain frozen in a given angular configuration for a long time.

In our simulations we measured a variety of quantities in the model as a function of α , β , the frustration parameter f (for $f=0$ and $f=\frac{1}{2}$), and also as a function of the lattice sizes and number of Monte Carlo steps (MCS)/site. The more relevant quantities amenable to experimental measurements are the helicity modulus (i.e., the superfluid density), the internal energy, and the specific heat.

The helicity modulus Υ measures the response of the system to a twist along a spatial direction, say the x direction. Adding an additional angle $k_0 x$ in the x direction, where $k_0 = 2\pi/\lambda_0$ and λ_0 is the wavelength of the twist, to the argument in the cosine of the Josepson contribution to the action \mathcal{A} of Eq. (3.20) the helicity modulus is then calculated by²⁴

$$\Upsilon = \left. \frac{\partial^2 \mathcal{F}}{\partial k_0^2} \right|_{k_0=0} \quad (4.1)$$

with \mathcal{F} the free energy associated with \mathcal{F}_0 , $\beta \mathcal{F} = -\ln(\mathcal{Z}_0)$. This quantity provides an excellent test of the physical properties of the system, since it is directly proportional to the superfluid density. From the explicit expression for the partition function given in Eqs. (3.19) and (3.20), and taking the derivatives with respect to k_0 and setting $k_0=0$, one obtains the discretized expression for the helicity modulus,

$$\begin{aligned} \frac{\hbar}{L^2 E_J} \Upsilon = & \frac{1}{L^2 L_\tau} \left[\left\langle \sum_{x,y,k} \cos[\varphi_{x+1}(\tau_k) - \varphi_x(\tau_k)] \right\rangle - \frac{E_J \beta}{L_\tau} \left\langle \left[\sum_{x,y,k} \sin[\varphi_{x+1}(\tau_k) - \varphi_x(\tau_k)] \right]^2 \right\rangle \right. \\ & \left. + \frac{E_J \beta}{L_\tau} \left\langle \left[\sum_{x,y,k} \sin[\varphi_{x+1}(\tau_k) - \varphi_x(\tau_k)] \right] \right\rangle^2 \right]. \end{aligned} \quad (4.2)$$

The Hamiltonian is an even function of the angular difference, so the last term vanishes in all configurations. We also calculated the internal energy per site, $E = \partial(\beta \mathcal{F})/\partial \beta$, which is equal to

$$\frac{1}{\hbar L^2} E = \frac{L_\tau}{2\beta \hbar} - \frac{1}{L^2 L_\tau} \frac{E_J}{\hbar} \left\langle \sum_{i,k} \{1 - \cos[\varphi_{i+1}(\tau_k) - \varphi_i(\tau_k)]\} \right\rangle + \frac{1}{L^2} \frac{\hbar}{\alpha E_J} \frac{L_\tau}{(\beta \hbar)^2} \left\langle \sum_{i,k} \{1 - \cos[\varphi_i(\tau_{k+1}) - \varphi_i(\tau_k)]\} \right\rangle, \quad (4.3)$$

on the discrete lattice. Note that the first term in the helicity modulus is proportional to the internal energy. The specific heat per site, $C_v/k = -\beta^2(\partial E/\partial \beta)$, was also calculated. The discrete expression is

$$\begin{aligned} \frac{1}{\hbar L^2 k_B} C_v &= \frac{L_\tau}{2\hbar} - \frac{2L_\tau \hbar}{\alpha E_J (\hbar \beta)} \left\langle \sum_{i,k} \{1 - \cos[\varphi_i(\tau_{k+1}) - \varphi_i(\tau_k)]\} \right\rangle \\ &+ \frac{(\beta \hbar)^2}{L^2} \left(\frac{E_J}{\hbar L_\tau} \right)^2 \sigma_x^2 + \frac{1}{L^2} \left(\frac{L_\tau \hbar}{\alpha E_J} \right)^2 \frac{1}{(\beta \hbar)^2} \sigma_\tau^2 + \frac{2}{\alpha \hbar L^2} \sigma_{x\tau}, \end{aligned} \quad (4.4)$$

when

$$\Phi_\tau = \sum_{i,k} \{1 - \cos[\varphi_i(\tau_{k+1}) - \varphi_i(\tau_k)]\}$$

and

$$\Phi_x = \sum_{i,k} \{1 - \cos[\varphi_{i+1}(\tau_k) - \varphi_i(\tau_k)]\}$$

we have defined

$$\sigma_x^2 = \langle \Phi_x^2 \rangle - \langle \Phi_x \rangle^2,$$

$$\sigma_\tau^2 = \langle \Phi_\tau^2 \rangle - \langle \Phi_\tau \rangle^2,$$

and

$$\sigma_{x\tau} = \langle \Phi_x \Phi_\tau \rangle - \langle \Phi_x \rangle \langle \Phi_\tau \rangle.$$

The expressions when $f_{i+1,i} \neq 0$, entail adding the $f_{i+1,i}$ term to the arguments of the sine and cosine functions.

The fact that C_v is not just given as the fluctuation of the internal energy is a consequence of the discretization along the τ axis. This would seem to imply a violation of the Callen-Welton-Kubo fluctuation-dissipation theorem. However, if we rewrite the above expression in terms of ϵ as defined in Eq. (3.6), and look at the limit $\epsilon \rightarrow 0$, recalling that in this limit

$$\{1 - \cos[\varphi_i(\tau_{k+1}) - \varphi_i(\tau_k)]\} \rightarrow \frac{\epsilon^2}{2} \left(\frac{\partial \phi}{\partial \tau} \right)^2,$$

one finds that the violations to the fluctuation-dissipation theorem are of $O(\epsilon)$. Thus it is recovered in the continuum limit.

We performed several checks of the algorithm described above. First, we checked that the QMC simulations of the 0-dimensional model were in agreement with the results discussed in the preceding section. The simulations were carried out in $2 \times 2 \times L_\tau$ lattices. For $L_\tau \geq 500$ and $N = 5000$ the results are essentially on top of the exact answers obtained from Eq. (3.3). Also, for the full model we checked that in the limit $\alpha \rightarrow 0$ our results compared successfully with previous calculations in the classical limit for the internal energy, the specific heat, and Υ .

We also tested our QMC results in the semiclassical limit against perturbative results obtained from the WKB approach described in Ref. 3. For the internal energy,

$$\frac{E}{E_J} = -2 + \frac{1}{2\beta E_J} + \frac{1}{(4\beta E_J)^2} + \frac{\alpha}{48} + \frac{\alpha}{198\beta E_J} + O(\alpha^2), \quad (4.5)$$

and the helicity modulus

$$\frac{\Upsilon}{(\alpha^2 E_J)} = 1 - \frac{1}{4\beta E_J} - \frac{\beta E_J \alpha}{24} - O(\alpha^2). \quad (4.6)$$

The first two terms in Eq. (4.6) are the ones obtained by

Ohta and Jasnow,²⁴ while the third term is the leading correction to lowest order in α .

In practice, in order to test the statistical accuracy of our results, we followed the usual procedure of separating our measurements into n groups of m iterations each and, assuming statistical independence of the samples, estimated the standard deviation of the mean of the n groups of averages. In order to obtain meaningful answers from this procedure, especially in the case of C_v , which is given in terms of average fluctuations, we always used $n, m \geq 150$. (In most cases $n = m = 200$ was used, although some runs were done for n, m as large as 1000 at the lowest temperatures studied.)

In our analysis of the α dependence of T_c , this quantity was estimated in two different ways. Following the reasoning of Refs. 24 and 17, T_c was determined as the temperature for which $\Upsilon(\beta) = 2/\pi\beta$. The first, less precise method to determine this intercept consisted in measuring Υ in the temperature range that would produce three or four values above and below the low $\Upsilon_0 = 2/\pi\beta$. An error-weighted least-squares fit to these data was then used to determine the intersection. The uncertainty in T_c was the (analytically propagated) uncertainty in the fit, corresponding to a conservative min-max error estimation. The second method, more precise, but also more time consuming, consisted of a repeated readjustment of β by interval halving; the direction of the shift being determined by whether the current mean value of Υ was smaller or larger than Υ_0 . The uncertainty in T_c following from this procedure was then obtained by direct min-max for the intersections of $\langle \Upsilon \rangle_\beta \pm \sigma(\langle \Upsilon \rangle_\beta)$ with Υ_0 .

We checked whether the system had thermalized by the usual procedure of comparing the values for a given quantity coming from different initial configurations. This is, of course, temperature dependent, but we found that 5×10^3 to 1×10^4 iterations were generally sufficient at all but the lowest temperatures where thermalization in some instances required upwards of 2×10^4 MCS/site. In the fully frustrated case, where the bulk of our analysis was done, the interesting physics takes place at modest temperatures, where thermalization does not present major difficulties.

V. RESULTS

After making a few general comments on the nature of our simulations, in this section we shall describe the results of our numerical analysis. We will begin by describing briefly our results for the unfrustrated case ($f=0$), and then present our analysis of the fully frustrated problem ($f = \frac{1}{2}$).

As mentioned above, the main technical difficulty encountered in the simulation of our model stems from the asymmetrical weighting of the two contributions to the ac-

tion. At low temperatures, where our main interest lies, thermalization of some initial states can be very slow. For this reason, it is crucial to the success of a Monte Carlo analysis of this model to choose initial configurations carefully. Of course, in order to ascertain whether the system has thermalized at a given temperature, it is necessary to study the evolution of initial states which are widely separated in state space; close to a phase transition, this implies using initial states which are very far from equilibrium. As a case in point, in Fig. 2 we show the evolution of the internal energy of two states as a function of the number of Monte Carlo steps per site (we shall often refer to this kind of simulation as representing the *time* evolution of a state). The results are for the $f=0$ model for $\alpha=0.3$ simulated at a very low temperature. The state with higher initial energy, closer to an equilibrium state at these temperatures, is one where spatial planes at each L_τ value are completely ordered, but completely uncorrelated

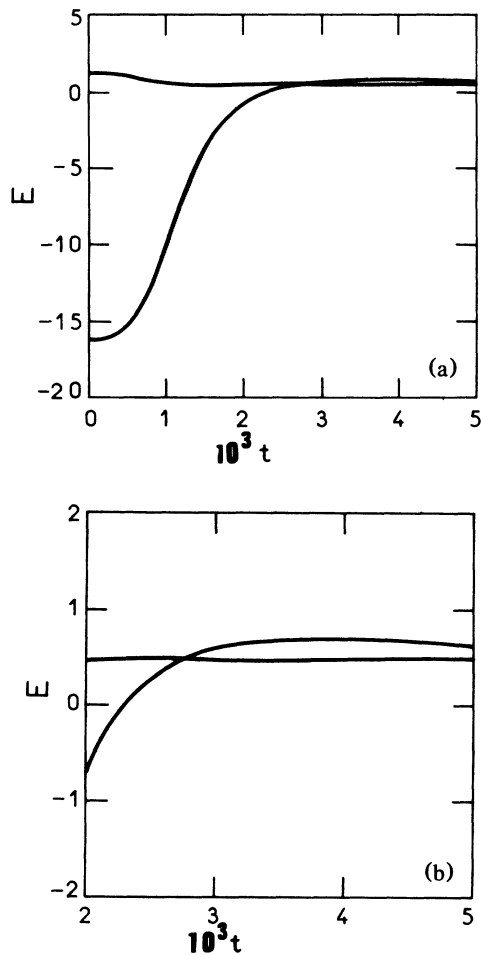


FIG. 2. (a) Time evolution of the energy of two different initial states close to a first-order transition in the $f=0$ problem for $\alpha=0.3$ at $T=0.02$. The abscissa is measured in MCS/site. The fluctuations in the simulation are smaller than the thickness of the smooth curve drawn over them. (b) Detail of (a) closer to the thermalized region. This figure shows two apparently stable states with different energies at $T=0.02$, signaling the presence of a nearby first-order transition.

from planes at different values of τ (in what follows we shall call this a *mixed-ordered* state). The other state, with lower initial energy, is ordered along the L_τ direction and completely disordered in each spatial plane (we shall refer to this state as a *mixed-disordered* state). Whereas the first state has essentially equilibrated after approximately 10^3 iterations, the second has taken about 4×10^3 iterations to reach its final state. This simulation, discussed in greater detail below, shows the existence of two apparently stable states with different energies at the same temperature, signaling the presence of a nearby first-order transition (further evidence supporting this contention, our main result, will be given later). In Fig. 3 we show the evolution of the same two initial states at a slightly higher temperature, where the energy gap has diminished. Note, however, that the mixed-disordered state has not yet thermalized after 5×10^3 iterations. Of course, our initial states will take less time to thermalize, and the situation is certainly less dramatic when far from a transition, but the above results clearly indicate that great care should be exercised in the region about T_{QUIT} . For the re-

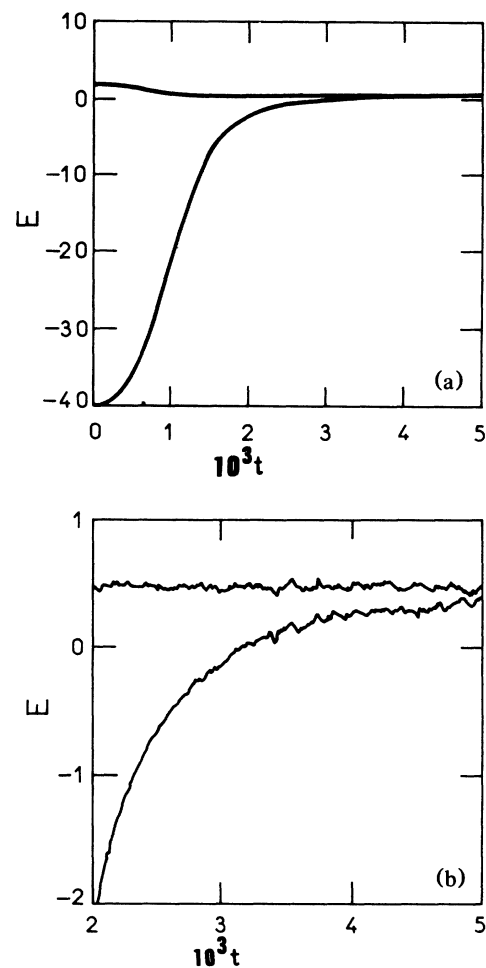


FIG. 3. (a) Time evolution of the same two states as shown in Fig. 2 but at a slightly higher temperature, $T=0.03$. (b) Same as (a) but closer to the equilibrium region. Note that the energy of the state with lower initial energy is still increasing after 5×10^3 iterations.

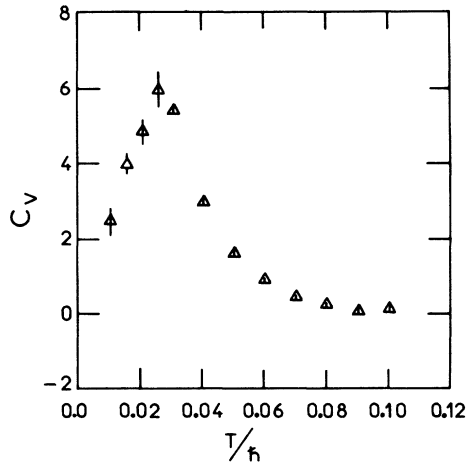


FIG. 4. The specific heat C_v vs temperature for $\alpha=0.3$ and $f=0$. Lattice sizes used in this simulation were $L \times L \times L_r$, with $L=10$, $L_r=150$ for $T \leq 0.024$ and $L=30$, $L_r=30$ for $T > 0.3$. At $T=0.03$ the simulation was done for both lattice sizes. The points below $T=0.03$ correspond to averages over $3-4 \times 10^5$ MCS/site after discarding 2×10^3 MCS/site. Error bars in this and in the following figures represent one standard deviation from the mean.

sults which follow, all initial states were thermalized for at least 5×10^3 iterations away from any phase transition, and for at least 10^4 iterations in the vicinity of a phase transition.

The existence of first-order transition in the model with $f=0$, implied by the above results, has been previously described.¹ Further evidence for the presence of this transition can be obtained from measurements of other thermodynamic variables. In Fig. 4 we display the specific heat as a function of the temperature for $\alpha=0.3$ and $f=0$. An apparent cusp (or discontinuity) in this quantity, typical of first-order transitions, is evident in the figure. It should be noted that the magnitude of the peak in C_v , for the size of the lattice studied, at T_{BKT} for $\alpha=0$ is of order one, whereas *here it is six times larger*. In Fig. 5 we show the results for the helicity modulus Y in the same temperature region. A striking discontinuity in Y can be seen at $T \approx 0.03$, roughly at the same place where the specific heat seems to have a cusp. Note, however, that unlike what would be expected in a reentrant transition, where $Y \rightarrow 0$ as $T \rightarrow 0$, here Y seems to tend to a finite value at $T=0$. This points to the existence of a hitherto unsuspected new coherent state in the model's very low temperature region. Because the temperatures at which this state appears are so low and, hence, from our previous discussion, the lattice sizes along the imaginary-time axis need to be so large, further analysis in this region is impractical. One would, for example, like to analyze the behavior of the model as a function of α , but such an endeavor would be prohibitively time consuming and was therefore not attempted. Also, to better ascertain the size dependence of C_v and Y at T_{QUIT} more calculations for different lattice sizes would be needed. However, given the large amount of computer time that was needed to get the points below T_{QUIT} shown in Figs. 4 and 5 [which was of the order of 70 central-

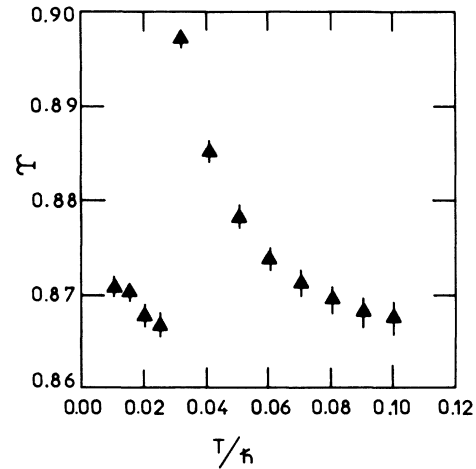


FIG. 5. The helicity modulus Y vs temperature for $\alpha=0.3$ and $f=0$. Lattice sizes and number of MCS/site were the same as those for Fig. 4.

processing-unit (CPU) hours on a Cray-XMP/48 super-computer] this analysis was not attempted.

Fortunately, as we shall discuss below, a related effect occurs in the presence of an external, transverse magnetic field, but at much higher temperatures. This makes a more complete analysis of the $f \neq 0$ case possible.

In the fully frustrated problem ($f = \frac{1}{2}$) the QUIT to this new state is much more evident than in the $f=0$ case. For comparison with Fig. 5, in Fig. 6 we display the results for the helicity modulus Y as a function of the temperature for $\alpha=0.3$ and $f = \frac{1}{2}$. A pronounced discontinuity with $\Delta Y \approx 0.1$ is evident around $T \approx 0.15$. Apart from the fact that this temperature is above five times larger than the corresponding $f=0$ value, here the gap in the helicity modulus is about thirty times larger. Another effect of the frustration is evident in Fig. 6. The rapid drop in Y , corresponding to the descendant of the BKT

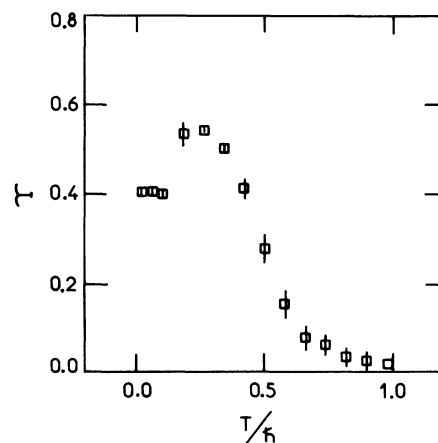


FIG. 6. The helicity modulus Y vs temperature for $\alpha=0.3$ and $f = \frac{1}{2}$. The lattice used in this simulation measured $8 \times 8 \times 30$. The values plotted correspond to averages over 4×10^4 MCS/site after discarding 10^4 MCS/site. Values were obtained by heating the mixed-order state described in the text.

transition of the classical $\alpha=0$, $f=\frac{1}{2}$ model, occurs at a temperature which is much closer to T_{QUIT} than it does in the $f=0$ case. We shall elaborate on this point at the end of this section.

A useful question to ask at this point is what type of fluctuations are responsible for this transition. A partial answer can be obtained by looking at the time evolution of the individual contributions to the internal energy at temperatures close to the transition. In Fig. 7 we plot the instantaneous value of the kinetic (charging) and potential (Josephson) contributions to the internal energy at $T=0.16$ for $\alpha=0.3$ and $f=\frac{1}{2}$. Starting from the mixed-ordered state described above a clear jump in the potential energy is seen after approximately 1.36×10^4 MCS/site. No such effect appears in the kinetic energy. This points clearly to the source of the QUIT being related to quantum fluctuations in the spatial correlations and not to correlations along the imaginary-time axis. Similar analyses of the separate contributions to the helicity modulus lead to the same conclusions. This plot distinctly shows the typical decay of a metastable state near a first-order transition.

It is important to review the physics of first-order transitions to understand how the cooling and warming branches of the thermodynamic quantities arise. Upon cooling from high temperatures only one state is allowed, thus increasing or decreasing the temperature does not change the stationary values for the thermally averaged quantities. Below the transition temperature there are two possible states. The lower free-energy state is more stable. However, the decay time for the metastable state to the equilibrium state can be very large and thus essentially unobservable in the time of an experiment. To reach the metastable state one may need to prepare the system appropriately. For example, to reach the glass state in a liquid one needs to cool the system quickly.

A similar situation exists in a simulation of a model that shows a first-order transition, in which one can find the competition between two different states. The dis-

tance on the free-energy surface between these two states may be very close to the transition temperature, leading to a longer lived metastable state at lower temperatures. In a liquid-crystal phase transition one is able to nucleate the crystalline phase more easily if a crystal "seed" is added to the system. Similarly, one should expect that we will be able to nucleate the metastable phase with more ease if we start from an initial configuration which is relatively close to that state on the free-energy surface. We have found this condition to be essential to see the QUIT. In fact, starting from the *mixed-ordered* state, say, the stable state may or may not appear (in a finite run, of course) depending on the initial seed for the random number generator (or using a different generator). This is not entirely surprising or unexpected in light of the above discussion; if the initial state is sufficiently far from the state of lowest free energy, and if the phase space available to this state is sufficiently small, it is quite easy for the system to freeze into one of the nearby metastable states. Simulation of systems with metastable states, as is well known, can be very subtle.

The size-dependence of the energy and helicity modulus near T_{QUIT} yields further information on the nature of the transition. In Fig. 8 we show the values of E and Υ near T_{QUIT} for three lattice sizes. At each temperature, the values of these quantities are seen to be independent, within the uncertainty of the measurement, of the size of the lattice. This is strong evidence of a first-order transition.

The hysteretic behavior implied in the above description of our results would be complete if it included a cooling branch as well. Unfortunately, we have not been able to see the full cooling branch in our simulations. This is not entirely surprising, since, as we have stressed in the preceding section, the efficiency of our algorithm decreases with temperature. Indeed, we have not been able to see the decay of a state in the cooling branch into a state in the heating branch. In Fig. 9 we have plotted both heating and cooling values for the internal energy and hel-

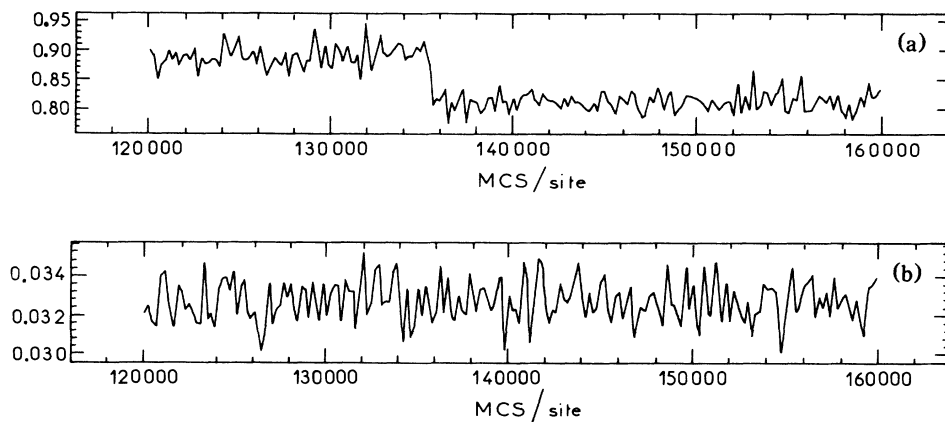


FIG. 7. The evolution of a mixed-ordered state, for $T=0.16$, $\alpha=0.3$, and $f=\frac{1}{2}$. Plotted are the individual contributions to the internal energy. The potential (or Josephson) term [graph (a)] shows a dramatic jump after $\approx 1.36 \times 10^5$ MCS/site, typical of the decay of a metastable state near a first-order transition. The kinetic (or charging) term [graph (b)], shows no such discontinuity. These results indicate that the origin of this first-order transition is related to spatial correlations and not to correlations along the imaginary-time axis.

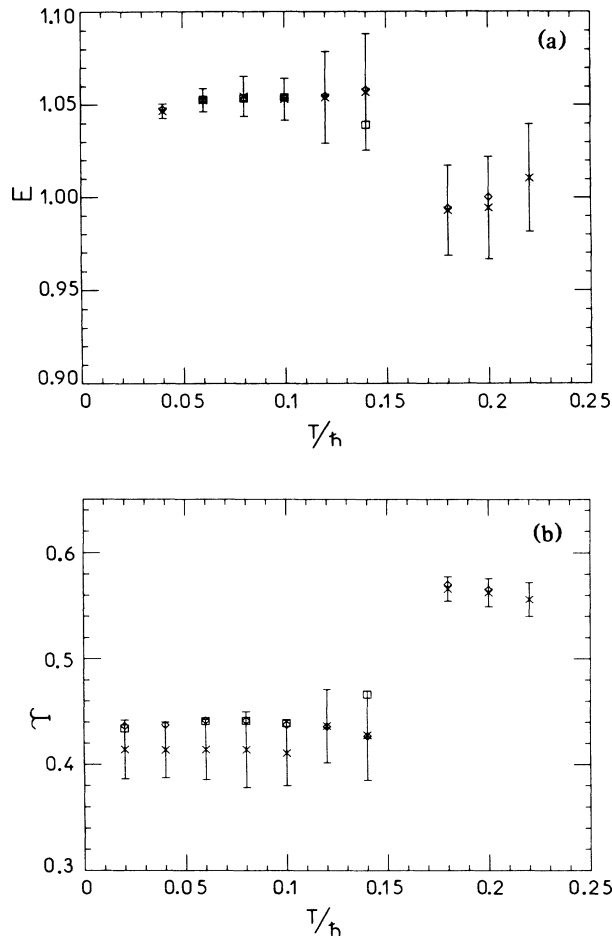


FIG. 8. (a) The internal energy E as function of the temperature for $\alpha=0.3$ and $f=\frac{1}{2}$. The values corresponding to three lattice sizes are plotted: $L \times L \times L_r$ with $L_r=30$ and $L=8$ (\times), $L=16$ (\diamond), and $L=24$ (\square). These results demonstrate that the energy is nearly independent of lattice size, a situation typical of first-order transitions. (b) Same as (a) but for the helicity modulus γ .

icity modulus. For temperatures above $T \approx 0.4$, both sets of values are seen to lie on top of one another.

The transition we have described occurs for a wide range of values of α . In Fig. 10 we display the heating branch for the internal energy as a function of temperature and for several values of α . For all values of α shown, the heating branches of both E and γ display a clear discontinuity at a temperature which increases very slowly with α . Although we have not determined this fact completely, it seems that the gap in both quantities disappears abruptly as α increases past $\alpha \approx 0.7$. We have also not been able to determine whether a minimum value of α exists below which the QUIT disappears. For the reasons given above, it is possible that the gap persists all the way down to $\alpha=0$ as long as the system is driven slowly to $\alpha=0$ from some nonzero value. In a similar manner, the existence of some nonanalyticity as a function of α might be used to explain the sudden disappearance of the gap for larger values of α . There are certainly interesting and important questions which should be answered. We shall not

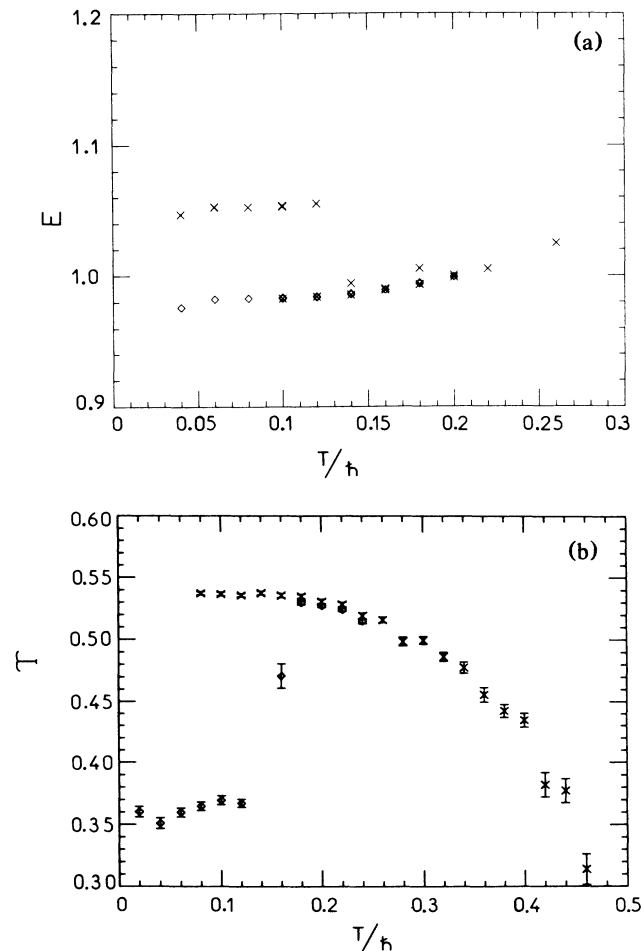


FIG. 9. (a) Cooling branch (\diamond) of hysteresis loop for the internal energy for $\alpha=0.5$, $f=\frac{1}{2}$. Lattice size was $8 \times 8 \times 30$. For temperatures above $T \approx 0.14$ values coincide with those of the heating (\times) branch. (b) Same as (a) but for the helicity modulus γ . In this figure we give the error bars as defined in the text.

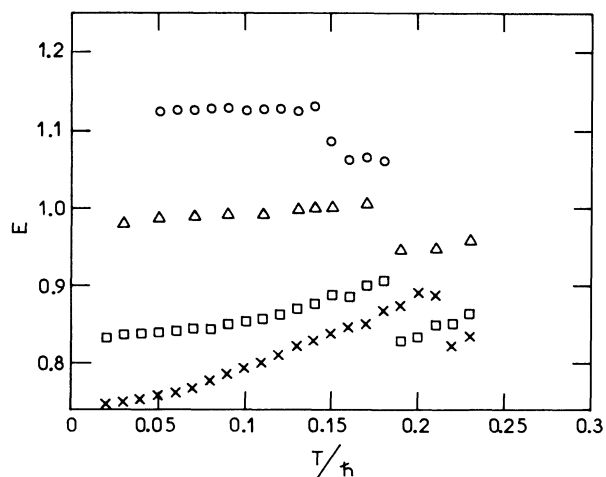


FIG. 10. The internal energy per site, E , as function of the temperature for several values of α : 0.01 (\times), 0.05 (\square), 0.2 (\triangle), and 0.5 (\circ). Here $L=8$ and $30 \leq L_r \leq 60$. After thermalization, averages were calculated over 55 K MCS/site.

dwel on this point any longer, but, as additional information, in Fig. 11 we present the results of a simulation performed at fixed temperature in the metastable region for several values of α and for $f = \frac{1}{2}$. The simulations were carried out starting with the two states at $\alpha = 0.3$, and successive points were obtained by lowering the value of α at fixed temperature. The most salient feature of these results is the fact that the gap between the heating and cooling values for both the internal energy as well as the helicity modulus does not show any clear trend as a function of α and, indeed, within the uncertainty of our measurement, seems to be very weakly dependent of α .

We have also analyzed the normal to superconducting transition which our model exhibits at moderate temperatures and which is the direct descendant of the transition in the classical, $\alpha = 0$ and $f = \frac{1}{2}$ model. The transition temperature in this case was determined, using the methods described in the preceding section, to be the point at which the helicity modulus intersects the BKT line given by $\Upsilon(T_c(f, \alpha)) = 2T_c/\pi$. This procedure is not completely justified theoretically, since we lack a full theory for the

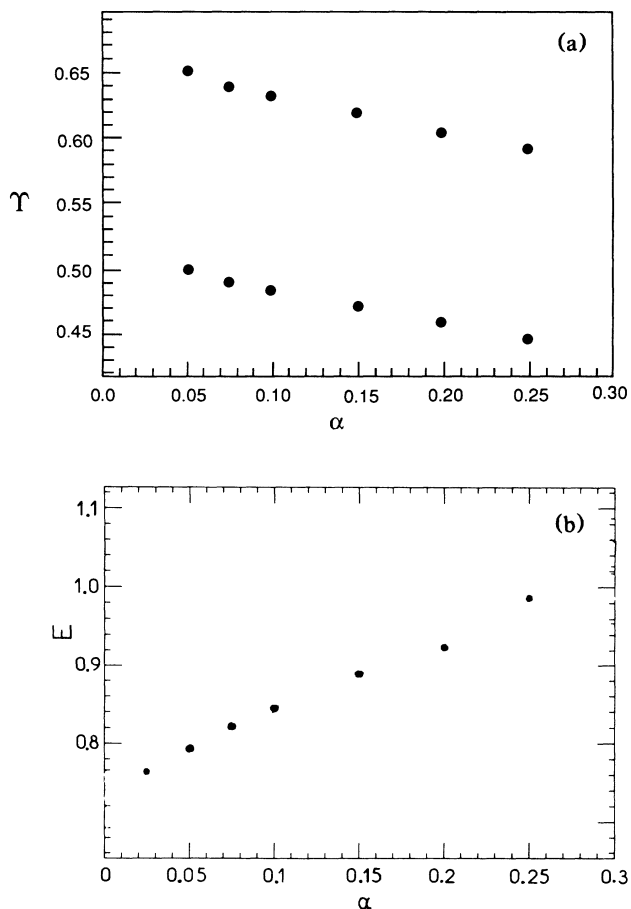


FIG. 11. (a) The helicity modulus in the metastable region ($T=0.1$) for $f = \frac{1}{2}$ has a function of α . Lattice size was $8 \times 8 \times 30$ and measurements represent averages over 16 K MCS/site. Plotted are values of Υ obtained by cooling (upper set of points) and heating (lower set). (b) Same as (a) but for the internal energy per site showing only the warming branch.

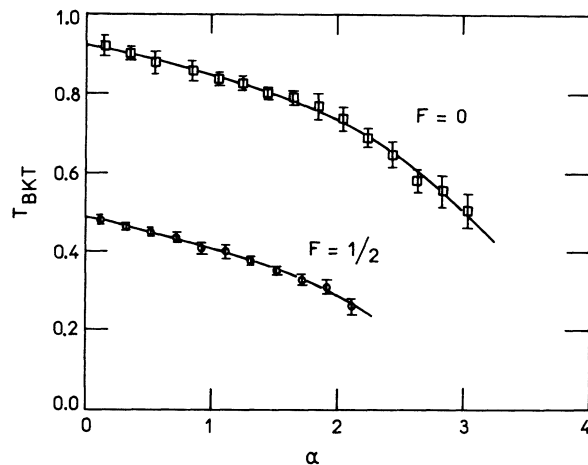


FIG. 12. $T_{\text{BKT}}(f=0)$ and $T_c(f = \frac{1}{2})$ as functions of α . Lattice sizes ($L \times L \times L_r$) were in the range $10 \leq L \leq 16$ and $30 \leq L_r \leq 60$. Each point on the graph was obtained, using the methods described in the text, from 10–12 measurements of Υ . Each value of Υ was obtained by averaging over 4×10^4 MCS/site.

frustrated case, even in the classical limit. However, it is possible to argue that, at least for $\alpha \ll 1$, $T_{\text{BKT}}(\alpha)$ and $T_c(\alpha, f = \frac{1}{2})$ should have a qualitatively similar behavior as functions of α . Indeed, within a WKB approximation,³ the contribution of the charging term in the action leads to a renormalization of the Josephson coupling; but the value of this coupling is determined solely by the fact that the Josephson contribution to the action is periodic. Since for nonzero f this term is also periodic, it follows that here the Josephson coupling should be renormalized in a way similar to the $f=0$ case.²⁵ Of course, this argument, valid for temperatures close to T_c , is only true for small α . The above caveat notwithstanding, it is reassuring that the α dependence of T_c , as obtained from the heuristic procedure we have described, is remarkably similar to that of T_{BKT} . In Fig. 12 we plot T_c and T_{BKT} as functions of α . An error-weighted least-squares cubic fit to the data gives

$$T_{\text{BKT}}(f=0) = 0.9265 - 0.0834\alpha + 0.0157\alpha^2 - 0.012\alpha^3, \quad (5.1)$$

$$T_c(f = \frac{1}{2}) = 0.4934 - 0.0952\alpha + 0.244\alpha^2 - 0.0147\alpha^3. \quad (5.2)$$

The fact that the coefficients of the above fits are small provides an *a posteriori* justification for our analysis.

VI. FABRICATION OF ULTRASMALL JUNCTION ARRAYS

To experimentally observe a QUIT of the type discussed above depends critically on the ability to fabricate arrays of Josephson junctions with suitably small capacitances. Existing technology may be adequate for this purpose depending on the specific range of capacitances re-

quired. It is certain that the smallest capacitances would be achieved in a granular system which characterizes thin films at the earliest stages of their growth. However, randomness in such systems may prove to be a drawback to quantitative comparisons between experiment and theory.

The closest geometry to that required to study the regime discussed here is very likely the 20000-junction array fabricated at IBM several years ago.²⁶ The all-Nb junctions were formed on an oxidized Si chip using electron-beam lithography. The geometry was that of crossed strips with an overlap area of $1 \mu\text{m}^2$. The capacitances of the junctions were estimated to be 0.1 ± 0.02 pF.

Unfortunately, the junctions described above probably have too large a capacitance to exhibit the effects discussed here. Capacitances at the level 1–10 fF may be achieved by using a two-layer electron-beam technique with Sn electrodes.²⁷ This has been done by using narrow (0.2–0.4- μm) in-line electrodes. The dielectric in these edge junctions, SnO_x , has a low dielectric constant, which helps to make low junction capacitances possible. These junctions have not yet been formed in array configurations.

Configurations with capacitances of the order of 0.07–0.03 fF have been produced by Fulton and Dolan,²⁸ but were not reported to exhibit Josephson effects. In part, this may be because they were not cooled to sufficiently low temperatures. These Al-Al junctions were formed using a multiple angle, deposition-oxidation-deposition cycle. In fact, the major problem in producing ordered arrays with capacitances smaller than the order of femtofarads may be the difficulty of ensuring the occurrence of the Josephson effect.

A more speculative approach, which could result in much lower capacitance junctions, but which runs the risk of not succeeding because the Josephson coupling may be too weak, is the use of the techniques of Kratschmer and Isaacson.²⁹ This involves the deposition of AlF_3 on a substrate and then writing directly on the surface with a high-intensity, finely focused electron beam. With appropriate dosage of electrons it is possible to form a checkerboard pattern of Al squares directly, where the spacing between squares is the order of 1–10 nm. The resultant tunneling junctions, if strongly enough coupled, would have capacitances of less than 0.1 fF. It might be possible to increase the tunneling coupling without substantially increasing the capacitance by forming these structures on doped substrates, or on substrates which are degenerate semiconductors. Although some structures have been discussed by Kratschmer and Isaacson, to our knowledge their superconducting properties have not been investigated.

VII. DISCUSSION

In this paper we have presented an extensive Monte Carlo study of the low-temperature properties of a model for a two-dimensional periodic array of ultrasmall Josephson junctions. The most important result emerging from our studies is that of finding strong evidence for the existence of a low-temperature ordered phase which is com-

pletely dominated by quantum fluctuations. The evidence for these quantum (-fluctuation-) induced (phase) transitions (QUIT's) has emerged from calculations of the helicity modulus, internal energy and to a lesser extent of the specific heat with and without a magnetic field. The effects of a QUIT are found to be more pronounced in the presence of the magnetic field.

One can discuss the properties of the model in the case $f=0$ in terms of the tentative phase diagram shown in Fig. 13. There we see that at zero temperature we should find the behavior of a 3D XY model with one critical point for a critical value of α , say α_c .¹¹ Below α_c , we expect to find long-range phase coherence as measured by the phase correlation functions. From the universal properties associated with the $T=0$ critical point, we can expect that at sufficiently low but finite temperatures around α_c the correlations should decay exponentially with distance as well.

At higher temperatures, close to $T_{\text{BKT}}(\alpha)$ we expect the correlation functions to decay algebraically with a renormalized $\eta(\alpha)$, and to have a line of fixed points just below $T_{\text{BKT}}(\alpha)$.³ The $T_{\text{BKT}}(\alpha)$ transition is produced by the unbinding of thermally excited vortices (TEV). It was found that as the temperature is lowered the quantum fluctuations have the effect of nucleating vortex pairs.³ We have called these quantum nucleated vortex pairs QEV. The appearance of QEV can be understood heuristically from our imaginary-time representation. When the temperature is high, around $T_{\text{BKT}}(\alpha)$, the world line of the vortex pairs are of the order of $\beta\hbar$, and thus the quantum fluctuations related to the displacements perpendicular to the τ direction cannot be large. When the temperature is lowered, $\beta\hbar$ and thus τ grow and therefore the possibility of creation and destruction of vortex pairs increases. It is for this reason that a perturbative analysis as a function of the vortex pair density breaks down at low temperatures.³

At intermediate temperatures we have the first-order

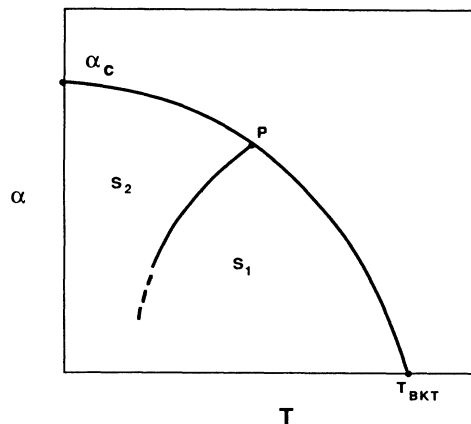


FIG. 13. Conjectured phase diagram for $f=0$. At $T=0$, α_c is the critical coupling of the anisotropic 3D XY model. Region S_1 denotes the renormalized BKT phase with power-law-decaying correlations. Around α_c at finite but low temperatures in region S_2 the correlations decay exponentially. The line that separates S_1 from S_2 denotes the first-order boundary dividing the superconductive S_1 and S_2 phases.

QUIT. A first-order transition has a finite correlation length. A question which arises is the understanding of how can one go from an ultralow exponential decay of correlations to an algebraic one, both characteristic of second-order phase transitions, passing by the first-order QUIT transition. Since the first-order region exists precisely for intermediate temperatures, neither weak- nor strong-coupling expansions can shed light into the physics around this transition, and therefore the need for the type of nonperturbative analyses given in this paper exists.

For the $f \neq 0$ case, the situation is still more complicated since we do not know for sure what the behavior of correlations at high or low temperatures is. In this case, a new type of vortex excitation appears, field-induced vortices (FIV), that can be distinguished from the TEV in that they can have fractional vorticity and will be present at all temperatures. In the fully frustrated case, fractional charged vortices are known to exist mainly in the ground state.^{14,17} Of course, the ground state of the model considered here is different due to the zero-point quantum fluctuations. In the case where there is an $f \neq 0$ we have present TEV, FIV, and QEV, and thus it remains as a subject for future study to understand how each one of these excitations participates in the triggering of the QUIT, and the nucleation of the low-temperature quantum fluctuation dominated superconducting phase. We leave the answering of some of these important theoretical questions for future studies.

ACKNOWLEDGMENTS

The calculations presented in this paper were carried out on Cray Research, Inc., Cray1 and Cray2 supercomputers from the University of Minnesota, as well as the Cray-XMP/48 supercomputer from the Pittsburgh Supercomputer Center. We thank the U.S. National Science Foundation (NSF) Office for Advanced Scientific Computing and the Supercomputer Center of the University of Minnesota for support. The partial support for this work by NSF Grants No. DMR-85-03085 (Minnesota) and No. DMR-86-40360 (Northeastern) is gratefully acknowledged. One of us (J.V.J.) thanks C. De Dominicis for the hospitality extended to him at the Service de Physique Théorique (Gif-sur-Yvette, France), where this paper was completed. He also thanks J. Choi and P. Wiegmann for useful discussions.

APPENDIX

In this Appendix we discuss the dependence of $Z_{\mathcal{R}}$ given in Eq. (3.13) for finite L_{τ} and with the angle $\phi \in [0, 2\pi]$ discretized into N equally spaced angles using the transfer-matrix technique. Define $x = 2L_{\tau}/\beta E_c$. Then the L_{τ} , N th approximation to the partition function is

$$Z_{L_{\tau}, N} = \frac{(x)^{L_{\tau}/2}}{N^{L_{\tau}}} \text{Tr}(\mathbf{A}^{L_{\tau}}), \quad (\text{A1})$$

where \mathbf{A} is an $N \times N$ transfer matrix with elements

$$a_{i,j} = \exp \left\{ x \left[\cos \left(\frac{2\pi(i-j)}{N} \right) - 1 \right] \right\}. \quad (\text{A2})$$

The matrix \mathbf{A} is a circulant, i.e., it can be written as

$$\mathbf{A} = \sum_{l=-R}^R c_l \mathbf{P}^l + c_{N/2} \mathbf{P}^{N/2}, \quad (\text{A3})$$

where the last term is present only if N is even. Here \mathbf{P} is the $N \times N$ permutation matrix

$$\mathbf{P} = \begin{pmatrix} 0 & 0 & 0 & \cdots & 1 \\ 1 & 0 & 0 & \cdots & 0 \\ 0 & 1 & 0 & \cdots & 0 \\ \vdots & & \ddots & \ddots & \vdots \\ 0 & 0 & \cdots & 1 & 0 \end{pmatrix}, \quad (\text{A4})$$

the coefficients are given by

$$c_l = \exp \{ x [\cos(2\pi l/N) - 1] \},$$

and $R = N/2 - 1$ if N is even and $(N-1)/2$ if N is odd. The eigenvalues of \mathbf{A} can now easily be written, since the eigenvectors and eigenfunctions of \mathbf{P} and hence of \mathbf{A} are known.³⁰ This gives

$$Z_{L_{\tau}, N} = \frac{1}{N^{L_{\tau}}} (x)^{L_{\tau}/2} \sum_{i=1}^N \lambda_i^{L_{\tau}}, \quad (\text{A5})$$

where the eigenvalues are given by

$$\lambda_i = \sum_{l=-R}^R c_l \cos \left(\frac{2\pi i l}{N} \right) + (-1)^i e^{-2x} \quad (\text{A6})$$

with the last term present only when N is even. Figures 1(d), 1(e), and 1(f) show, respectively, the comparison of the free energy, internal energy, and specific heat for fixed $L_{\tau} = 10^3$ and various values of N . See Sec. III for the significance of these figures.

*Present address.

¹L. Jacobs, J. V. José, and M. A. Novotny, Phys. Rev. Lett. **53**, 2177 (1984).

²L. Jacobs, J. V. José, M. A. Novotny, and A. Goldman, Europhys. Lett. **3**, 1295 (1987).

³J. V. José, Phys. Rev. B **29**, 2836 (1984).

⁴R. A. Webb, R. Voss, G. Grinstein, and P. Horn, Phys. Rev. Lett. **51**, 690 (1983); W. Abraham, C. J. Lobb, and M. Tinkham, Phys. Rev. B **28**, 6578 (1983); Ch. Leemann, Ph.

Derch, G. Racine, and P. Martinoli, Phys. Rev. Lett. **56**, 1291 (1986).

⁵B. Abeles, P. Sheng, M. D. Couttsan, and Y. Arie, Adv. Phys. **24**, 407 (1975).

⁶E. Simanek, Solid State Commun. **31**, 419 (1979); Phys. Rev. B **32**, 500 (1985); **23**, 5726 (1981).

⁷K. B. Efetov, Zh. Exp. Teor. Fiz. **78**, 2017 (1979) [Sov. Phys. JETP **51**, 1015 (1980)].

⁸P. Fazekas, Z. Phys. B **45**, 215 (1982); Y. Imry and M. Stron-

- gin, Phys. Rev. B **24**, 6353 (1981).
- ⁹D. M. Wood and D. Stroud, Phys. Rev. B **25**, 1600 (1982).
- ¹⁰M. Schroter, P. Fazekas, and B. Mühlischlegel, Z. Phys. B **57**, 193 (1986); R. Fazio and G. Giaquinta, Phys. Rev. B **34**, 4909 (1986).
- ¹¹S. Doniach, Phys. Rev. B **24**, 5063 (1981).
- ¹²D. U. Gubser, S. Wolf, W. W. Fuller, D. Van Vechtan, and R. W. Simon, Physica **135B**, 131 (1985), Phys. Rev. B **36**, 1962 (1988).
- ¹³J. M. Kosterlitz and D. Thouless, J. Phys. C **6**, 1181 (1983); V. L. Berezinskii, Zh. Theor. Fiz. **59**, 907 (1970) [Sov. Phys. JETP **34**, 610 (1971)].
- ¹⁴W. Y. Shi and D. Stroud, Phys. Rev. B **28**, 6575 (1983); **30**, 6774 (1984); **32**, 158 (1985); M. Y. Choi and S. Doniach, *ibid.* **31**, 4516 (1985); T. H. Halsey, *ibid.* **31**, 5728 (1985); M. Yosefin and E. Domany, *ibid.* **32**, 1778 (1985).
- ¹⁵B. Pannetier, J. Chaussy, R. Rammal, and C. V. Villegier, Phys. Rev. Lett. **53**, 1845 (1984).
- ¹⁶J. Villain, J. Phys. C **10**, 4793 (1977); E. Fradkin, B. Huberman, and S. Shenker, Phys. Rev. B **18**, 4789 (1978); J. V. José, *ibid.* **20**, 2167 (1979); in *Proceedings of the Kyoto Summer Institute, 1979*, edited by Y. Nagaoka and S. Hikami [Prog. Theor. Phys. **127** (1979)]; C. Ebner and D. Stroud, Phys. Rev. B **31**, 165 (1985); S. John and T. C. Lubensky, *ibid.* **34**, 4815 (1986).
- ¹⁷S. Teitel and C. Jayaprakash, Phys. Rev. Lett. **51**, 1999 (1983); Phys. Rev. B **27**, 598 (1983).
- ¹⁸B. Berge, H. J. Diep, A. Ghuzali, and P. Lallemand, Phys. Rev. B **34**, 3177 (1986).
- ¹⁹B. Jeanneret, Ch. Leemann, and P. Martinoli, in *Proceedings of the Eighteenth International Conference on Low-Temperature Physics* [Jpn. J. Appl. Phys. **26**, 1999 (1987)].
- ²⁰C. Lobb, D. W. Abraham, and M. Tinkham, Phys. Rev. B **27**, 150 (1983).
- ²¹B. G. Orr, H. M. Jaeger, A. M. Goldman, and C. G. Kuper, Phys. Rev. Lett. **56**, 378 (1986).
- ²²J. Tobochnik and G. V. Chester, Phys. Rev. B **20**, 3761 (1971).
- ²³N. Metropolis, A. W. Rosenbluth, M. N. Rosenbluth, A. H. Teller, and E. Teller, J. Chem. Phys. **21**, 1087 (1953); K. Binder, *Monte Carlo Methods*, Topics in Current Physics, Vol. 7 (Springer-Verlag, Heidelberg, 1979); M. Creutz, L. Jacobs, and C. Rebbi, Phys. Rep. **95**, 201 (1983).
- ²⁴T. Ohta and D. Jasnow, Phys. Rev. B **20**, 139 (1979).
- ²⁵M. Y. Choi and D. Stroud, Phys. Rev. B **32**, 7173 (1985).
- ²⁶R. F. Voss and R. Webb, Phys. Rev. B **25**, 3446 (1982).
- ²⁷M. Iansiti *et al.*, Phys. Rev. Lett. **59**, 489 (1987); E. L. Hu, L. D. Jackel, and R. E. Howard, IEEE Trans. Electron Devices **ED-28**, 1382 (1987), and references found therein.
- ²⁸T. A. Fulton and G. J. Dolan, Phys. Rev. Lett. **59**, 109 (1987), and references therein.
- ²⁹E. Kratschmer and M. Isaacson, J. Vac. Sci. Technol. B **4**, 361 (1986).
- ³⁰M. Marcus and H. Minc, *A Survey of Matrix Theory and Matrix Inequalities* (Allyn and Bacon, Boston, 1964), p. 65.